

Control Optimization for Parametric Hamiltonians by Pulse Reconstruction

Piero Luchi^{1,2}, Francesco Turro^{1,2}, * Xian Wu³, Sofia Quaglioni³, Valentina Amitrano^{1,2}, Kyle Wendt³, Jonathan L Dubois³, and Francesco Pederiva^{1,2}

¹*Physics Department, University of Trento, Via Sommarive 14, I-38123 Trento, Italy*

²*INFN-TIFPA Trento Institute of Fundamental Physics and Applications, Via Sommarive 14, I-38123 Trento, Italy and*

³*Lawrence Livermore National Laboratory, P.O. Box 808, L-414, Livermore, California 94551, USA*

Optimal control techniques provide a means to tailor the control pulse sequence necessary for the generation of customized quantum gates, which help enhancing the resilience of quantum simulations to gate errors and device noise. However, the substantial amount of (classical) computing required for the generation of customized gates can quickly spoil the effectiveness of such an approach, especially when the pulse optimization needs to be iterated. We report the results of device-level quantum simulations of the unitary (real) time evolution of the hydrogen atom, based on superconducting qubit, and propose a method to reduce the computing time required for the generation of the control pulses in the hypothetical case in which the hydrogen Hamiltonian depends parametrically on a time-varying effective electron mass. We use two simple interpolation schemes to accurately reconstruct the control pulses sequence starting from pulses obtained for a discrete set of pre-determined electron mass values, by finding the mathematical relation between them. We obtain a reconstruction with very high fidelity and a substantial reduction of the computational effort.

I. INTRODUCTION

The standard quantum computing (QC) approach is based on expressing arbitrary unitary operations in terms of a set of universal (or primitive) quantum gates, making use of the Solovay-Kitaev theorem [1]. This gate-based approach has been demonstrated to be, in principle, efficient for the simulation of complex systems on a quantum computer [2, 3]. In practice, the performance and reliability of the generated real-time evolution suffer from gate error rates and quantum device noise. In fact, the decomposition of the unitary operator can consist of a large number of gates, giving rise to a deep circuit in which the sum of the individual quantum gate errors spoils the result. In addition to extending the coherence time by improving the manufacturing process and the design of available qubits [4–6], a less explored route to improve the noise-resilience of quantum simulations consists in designing efficient quantum control protocols that allow the implementation of arbitrary quantum gates. This control-based approach tailors a microwave control pulse such that, applied to the qubits or, subsets of them, realizes the desired unitary transformation in a minimal number of applications. [7–11]. This approach obtains both a shallower quantum circuit and a reduction in the noise that deep circuits produce. The mathematical framework in which we operate is quantum optimal control [12–14], defined as the procedure of designing microwave pulses that perform arbitrary unitary transformations using nonlinear optimization techniques.

The quantum optimal control approach is very useful to simulate quantum mechanical systems where the standard gate-based approach performs poorly because of the need of very deep quantum circuits, with the consequence

of generating large cumulative error rates [15]. However, the control-based approach is not flawless. The optimization process requires a substantial amount of classical computational power and time, which grows quickly with the dimensionality and complexity of the simulated system. Moreover, if the targeted unitary operator depends on some external or internal time-dependent parameter, the control signal needs to be recomputed at each simulation time-step. This drawback can be effectively addressed by finding a way to parametrize and reconstruct the control pulses, thereby avoiding a full re-evaluation for each realization of the time-dependent parameters. In this paper, we propose a method to reconstruct such control pulses for parametric Hamiltonians starting from a limited set of such control pulses, coming from a discrete set of points in the Hamiltonian parameters space, using some simple fitting procedures. This protocol is applied and tested in the simulation of the $1s$ electron wavefunction of an Hydrogen atom, expanded in a standard computational chemistry basis set [16]. We test the method on the hypothetical case in which the Hamiltonian of the hydrogen atom depends parametrically on a time-varying effective mass of the electron, m_e . The control pulses providing the real-time propagator for a fixed time interval is evaluated for some arbitrary values of m_e starting from a finite set of controls, computed in advance, using two different interpolation method. The first is based on the interpolation of the coefficients of a polynomial fit of the control pulses, while the second is based on the interpolation of the spectra relative to the control pulses. This second method is able to deal with control pulses with a broad range of frequency components and is the one on which we focus the most, while the first is intended primarily to explain the idea behind the methods. In all cases, however, this reconstruction approach has proven to be able to obtain high-fidelity optimal control pulses with a reduced computational cost.

In this work, we test our reconstructing method at

* piero.luchi@unitn.it

a device-simulation level taking as test case a multi-level superconducting circuit quantum electrodynamic (cQED) system [9, 11] given by a transmon [17, 18] coupled to the resonant mode of a microwave cavity [19]. Moreover, the microwave control pulses driving the transmon were obtained with an optimization algorithm known as Gradient Ascent Pulse Engineering (GRAPE) [20, 21]. Quantum optimal control techniques are, however, a very general tool which are, in principle, applicable to any hardware. One only need to take into account the specific characteristics of the quantum device in the specification of the parameters needed in the optimization procedure.

The structure of the present work is the following. A brief description of the quantum system under study, of the adopted superconducting circuit and of the optimization algorithm can be found in Sec. II. A general description of the control pulses reconstructing method is presented in Sec. III. A simple interpolation method for the reconstruction of the control pulses and the analysis of the corresponding results are described in Sec. IV. Sec. V presents the Fourier transform reconstruction method and a simple example of its use. Finally, considerations on the scaling of the method are reported in Sec. VI, while conclusions are drawn in Sec. VII.

II. DEVICE HAMILTONIAN AND OPTIMIZATION PROCEDURE

The s-wave Hydrogen atom in spherical coordinates is given by:

$$H_{hy} = \left[-\frac{\hbar^2}{2m_e} \left(\frac{d^2}{dr^2} + \frac{2}{r} \frac{d}{dr} \right) - \frac{e^2}{r} \right], \quad (1)$$

were \hbar , and e are, respectively, the reduce Planck constant and the electron charge, here used in the atomic units (and so, from now on, set to 1 unless otherwise specified) and m_e is the electron mass, also expressed in atomic unit.

Given the Schrödinger equation:

$$i\hbar \frac{\partial |\psi_t(x)\rangle}{\partial t} = H_{hy} |\psi_t(x)\rangle, \quad (2)$$

the state of the hydrogen's electron is given by its formal solution, namely:

$$|\psi_{\Delta t}(r)\rangle = e^{-\frac{i}{\hbar} \Delta t H_{hy}} |\psi_0(r)\rangle = U_{\Delta t} |\psi_0(r)\rangle. \quad (3)$$

where $U_{\Delta t}$ is the unitary short-time evolution operator of the system, or propagator, i.e the unitary transformation we want to implement in the quantum device.

In order to solve the dynamics of the electron with a quantum device, we expand the electron orbital on a set of basis functions, the STO-KG basis, following the standard procedures used in computational chemistry [16], obtaining:

$$|\psi(r)\rangle = \sum_{i=1}^K A_i \phi(r; \alpha_i), \quad (4)$$

where A_i and α_i are numerical parameters (See. Tab VI) and $\phi(r; \alpha_i)$ are Gaussian basis function.

Now, we can obtain a numerical approximation of the hydrogen Hamiltonian computing the expectation $H_{i,j} = \langle \phi(r; \alpha_i) | H_{hy} | \phi(r; \alpha_j) \rangle$, for $i, j \in 0, K$. Finally we can numerically solve the Schrödinger equation. Further information about this basis expansion are presented in the Appendix A.

To study the real-time propagation of the Hydrogen system we follow the usual procedure for quantum simulation which consists in mapping the state of the system we want to simulate onto the levels of the quantum device [9, 11]. In particular, we map each STO-KG basis function on a level of our quantum device. In this way, the time-dependent occupation probabilities of the qubit's levels will correspond to the probability to find the electron in each of the basis elements.

We now introduce the general Hamiltonian of the quantum device, used as test, and on which we map the hydrogen system.

The Hamiltonian for a set of N superconducting quantum circuits in the dispersive regime (transmon regime) in the limit of low nonlinearity α coupled with a cavity [22] can be described by an appropriately parametrized Jaynes-Cumming model [23]:

$$H_d(t) = \sum_{k=1}^N \left(\omega_k b_k^\dagger b_k + \alpha_k b_k^\dagger b_k^\dagger b_k b_k + g_k (a b_k^\dagger + a^\dagger b_k) \right) + \omega_r a^\dagger a, \quad (5)$$

where $b_k^\dagger (b_k)$ are the creation (annihilation) operator for the transmon, $a^\dagger (a)$ are the creation (annihilation) operator for the cavity, ω_r is the frequency of the cavity, ω_k are the frequencies of the transmons and g_k are the coupling strength between each transmon and the cavity. In general, each transmon has more than two quantum levels, hence formally is not a standard qubit and, from now on, we identify it with the term "qudit". This quantum device can be controlled by irradiating each qudit with a resonant microwave pulse. This drive term is expressed as:

$$H_k^c(t) = \mathcal{E}_k(t) \cos(\omega_k^c + \phi_k) (b_k + b_k^\dagger), \quad (6)$$

where $\mathcal{E}_k(t)$ are the low-frequency envelopes of the microwave drive and ω_k^c are the carrier frequencies with phase offset ϕ_k . As a consequence, the complete Hamiltonian of the system is:

$$H(t) = H_d + \sum_{k=1}^N H_k^c(t) = \sum_{k=1}^N \left(\omega_k b_k^\dagger b_k + \alpha_k b_k^\dagger b_k^\dagger b_k b_k + g_k (a b_k^\dagger + a^\dagger b_k) + \mathcal{E}_k(t) \cos(\omega_k^c + \phi_k) (b_k + b_k^\dagger) \right) + \omega_r a^\dagger a. \quad (7)$$

Parameters	Values (GHz)
$\delta_r/(2\pi)$	0.4
$\delta_1/(2\pi)$	0.0
$\delta_2/(2\pi)$	-0.67
$g_1/(2\pi)$	0.1
$g_2/(2\pi)$	0.1
$\alpha_{1,2}/(2\pi)$	-0.32

TABLE I: Values of the parameters of the Hamiltonian in Eq. (8) for two qudits [13]. These are typical values for the dispersive regime in circuit QED

Finally, working in the rotating frame of the ground-state energy transition of the first qudit and applying the rotating wave approximation, the Hamiltonian takes the form:

$$H(t) = \sum_{k=1}^N \left(\delta_k b_k^\dagger b_k + \alpha_k b_k^\dagger b_k^\dagger b_k b_k + g_k (a b_k^\dagger + a^\dagger b_k) + \epsilon_I^k(t) (b_k + b_k^\dagger) + i \epsilon_Q^k(t) (b_k^\dagger - b_k) \right) + \delta_r a^\dagger a \quad (8)$$

where $\delta_r = \omega_r - \omega_1$ is the detuning of the cavity from the principle (carrier) drive frequency of the controls, and $\delta_k = \omega_k - \omega_1$ are the detuning of the transmons. Some typical values for this parameters are reported in Tab. I. $\epsilon_I^k(t)$ and $\epsilon_Q^k(t)$ are the in-phase and quadrature components of the drive pulse [11, 23] that the control-based quantum computing approach optimizes in order to simulate quantum systems.

For the sake of simplicity, we make two assumption which, however, do not reduce the generality of the method. First, we will perform explicit calculation considering only a single qudit. Second, we will neglect the terms associated to the cavity since the control pulse's principal frequency components, which drive the qudit, are highly detuned from the cavity frequency. Given these simplifications, the Hamiltonian reads:

$$H(t) = H_d + H_1^c(t) = \delta b^\dagger b + a b^\dagger b^\dagger b b + \epsilon_I(t) (b + b^\dagger) + i \epsilon_Q(t) (b^\dagger - b). \quad (9)$$

The transmon can be driven to simulate the real-time evolution with short-time propagator $U_{\Delta t}$ of the hydrogen system by appropriately optimizing $\epsilon_I(t)$ and $\epsilon_Q(t)$. For a given digital-time step Δt we use the GRAPE algorithm [13, 20, 21] to optimize the control sequences $\epsilon_I(t)$ and $\epsilon_Q(t)$ such that they satisfy, within a predetermined accuracy threshold, the equality:

$$U_{\Delta t} \equiv \exp \left(-i \hat{H}_{hy} \Delta t \right) \simeq \mathcal{T} \exp \left\{ -i \int_0^\tau \left[\hat{H}_d + \hat{H}_c(\tau') \right] d\tau' \right\} \quad (10)$$

where $\mathcal{T} \exp \{ \}$ stands for time-ordered exponential and τ is the total duration of the control pulse. The left-hand side of equation (10) correspond to the short-time propagator we want to simulate, while the right-hand side is the propagator induced on the transmon by the control pulses ϵ_I and ϵ_Q .

III. CONTROL PULSE RECONSTRUCTION (CPR) METHOD

There are two main drawbacks in the use of optimization algorithms (as GRAPE) to compute optimized control sequences: the large computational cost and the general non-transferability of the generated optimized controls, meaning that any change in the unitary operator requires a completely new optimization. This holds if there is any parametric dependence of the Hamiltonian, and a study of the system is required as a function of the parameter value. One example is the simulation of a scattering process of two nucleons interacting trough a spin/isospin dependent interaction, as captured by the leading order (LO) in the chiral effective field theory expansion. As described in Ref. [9] for the case of two neutrons, it is possible to break up the propagator in a spin-independent and a spin-dependent part, the latter being parametrically dependent on the instantaneous specific value of the coordinates of the neutrons. This implies that the control pulses implementing the instantaneous spin dynamics have to be computed at every time-step of the neutron's physical trajectory. This tends to neutralize the benefits in terms of computational speed-up that quantum computation allows in the simulation of quantum processes.

An explicit computation of the pulses for each value of the parameters can be avoided using the following general control pulse reconstruction (CPR) method. Given an Hamiltonian $H(\Lambda)$, where $\Lambda = [\lambda_1, \lambda_2, \dots, \lambda_K]$, is a point in the K -dimensional space of parameters characterizing the Hamiltonian, and assuming that one wants to implement on the quantum device the unitary transformation $U_{\Delta t}(\Lambda) = \exp \{ -i \Delta t H(\Lambda) \}$, one should:

1. Solve Eq. (10) (using GRAPE or some other equivalent optimization algorithm) for a discrete set of values of Λ and store the resulting control pulses. This results in obtaining a discrete set of controls each of which implements the specific unitary transformation for a certain value of Λ .
2. Perform a fit of the pulses either in terms of a function (e.g. a polynomial fitting) or as an expansion over a basis (e.g. Fourier transform of the pulses). Let us call $C = [c_1, c_2, \dots, c_M]$ the M coefficients of the fit (e.g. the polynomial coefficient or some type of coefficient relative to the expansion over a basis).
3. Find a mathematical relationship $C(\Lambda) = [c_1(\Lambda), c_2(\Lambda), \dots, c_M(\Lambda)]$ between the coefficients of

fit C and the parameters Λ of the unitary transformation $U(\lambda_1, \dots, \lambda_K)$.

4. Reconstruct the pulses for an arbitrary $\tilde{\Lambda}$ via the following procedure: select the $\tilde{\Lambda}$ values of interest, recover the fit parameters \tilde{C} through the mathematical relationship $C(\Lambda)$ and reconstruct, finally, the control pulses identified by \tilde{C} .
5. Repeat point 4 in the simulation loop to recover all the needed control pulses.

IV. APPLICATION: SIMPLE PULSE FITTING PROCEDURE

In this section a simple kind of parametric dependence of the Hydrogen short-time propagator will be presented. We expand the system Hamiltonian on the STO-2G basis and we use a single parameter dependence for the propagator, i.e. $U_{\Delta t}(\Lambda) = U_{\Delta t}(\lambda_1)$.

In general, the metric used to test our method is the fidelity Φ of the short-time propagator [21]:

$$\Phi = \langle U_{ex} | U_{rec} \rangle \langle U_{rec} | U_t \rangle \quad (11)$$

where $\langle U_{ex} | U_{rec} \rangle$ is the Hilbert-Schmidt inner product

$$\langle U_{ex} | U_{rec} \rangle = \frac{\text{Tr}\{U_{ex}^\dagger U_{rec}\}}{\dim(U_{ex})} \quad (12)$$

between the exact short-time propagator U_{ex} , computed directly via the left-hand side of Eq. (10), and the reconstructed short-time propagator U_{rec} , obtained plugging the optimized control pulses in right-hand-side of Eq. (10). Here $\dim(\cdot)$ represents the dimension of the propagator matrix. This provides a quantitative measure of the equivalence of the two unitary operators: Φ is equal to 1 when the operators are equal (i.e. they produce the same transformation) and is equal to zero when they are completely uncorrelated.

In this example, we choose as Λ the electron mass for the Hydrogen atom introduced in Sec. III, i.e. $\Lambda = \lambda_1 = m_e$, namely:

$$U_{\Delta t}(\lambda_1) \equiv U_{\Delta t}(m_e) = e^{-i\Delta t H_{hy}(m_e)}, \quad (13)$$

where we take $\Delta t = 1$ Hartree $^{-1}$. We seek control pulses solutions of 50 ns in duration (well below the typical coherence time of superconducting qubits [24]) with a sampling rate of 64 GHz (so the control is subdivided in 1600 time-steps). We solve the optimization problem of Eq. (10) using the quantum toolbox in Python (QuTip) package [25]. Specifically, we employ the GRAPE algorithm with the L-BFGS-B optimization method within the QuTip function `optimize_pulse_unitary`.

We follow the steps outlined in Sec. III:

- 1) We start by calculating the control pulses corresponding to an equally spaced sequence of the parameter m_e , with a required fidelity Φ between the computed

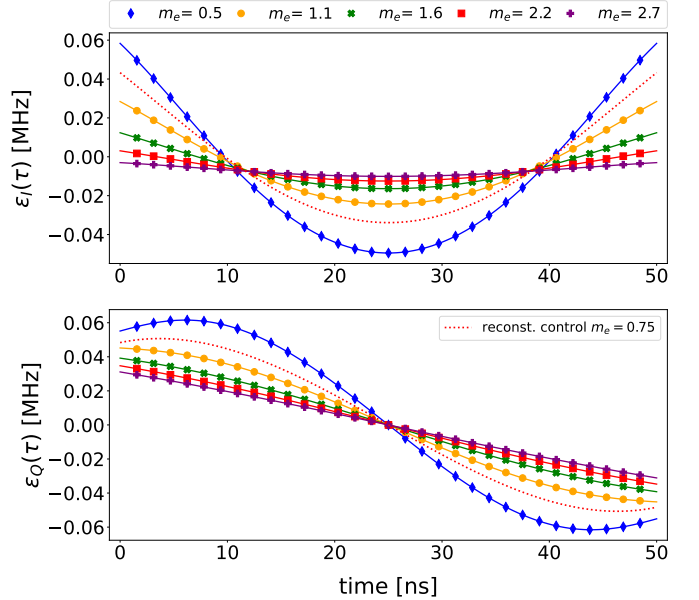


FIG. 1: Control pulses of the short-time propagator for the 1s orbital of the hydrogen atom expanded in the STO-2G basis set. Different curves correspond to different values of m_e . Upper panel: ϵ_I (in-phase component of the signal). Lower panel: ϵ_Q (in-quadrature component of the signal). The dotted line is the reconstructed control for an arbitrary value of m_e computed via the CPR method. As expected, it lays in between the controls for a greater and smaller value of m_e .

and target propagator of 0.99999. That is, we take a mesh of a certain interval of m_e and we compute, for each value, the associated control pulse, storing the results. Examples of control pulses are shown in Fig. 1. The initial guess for the first control pulse is the zero function. After that, to ensure that the obtained pulses are a continuously varying family of functions, the initial guess for the control optimization at a given value of m_e^i is taken to be the solution for the previous step, m_e^{i-1} . In this way the solution of the optimization problem remains in the neighbourhood of the same local minimum. Using the same (or a random) initial guess for different values of m_e^i , the solutions returned by the optimization algorithm can, in general, correspond to different local minima in the manifold of all the possible control pulses, giving rise to discontinuities that are undesirable for our present scope. The controls presented in this work are general and, in particular, there are no constraints on their initial and final values. Actually, in some contexts, the controls ending points are required to be zero to avoid unwanted transient produced by the wave generating device in the actual experimental setup. In practical terms, the quantum device is not affected by this lack. In the first place, the transient caused by the wave generating device is negligible with respect to the total duration of

the control. Secondly, the very high frequency transient that, in the physical device, corresponds to the non-zero initial values of the control pulses, does not affect the dynamics of the quantum device since, due to its quantum nature, it can be excited only by specific frequencies. However, the here presented CPR method is general and can be profitably used with any shape or type of control pulses.

2) In the second step, the control pulses $\epsilon_I(t)$ and $\epsilon_Q(t)$ are fitted with N^{th} degree polynomials $y_I(t)$ and $y_Q(t)$, namely:

$$y_{I(Q)}(t) = \sum_{j=0}^N c_j^{I(Q)} t^j, \quad (14)$$

where $c_j^{I(Q)}$ are the polynomial coefficients of $y_{I(Q)}(t)$ and t is the time in nanoseconds. Fig. 2 shows the distribution of the coefficients c_j^Q of $y_Q(t)$ for $N = 4$ as a function of m_e . These are mathematically the C parameters defined in Sec. III. The coefficients have a simple distribution that can be described by a low degree polynomial.

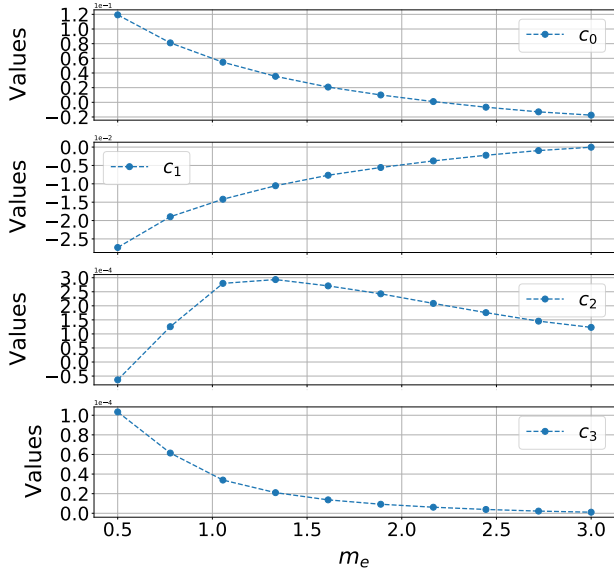


FIG. 2: Coefficients of the 4th degree polynomial fit (Eq. (14)) of the pulses in Fig. 1 as a function of the parameter m_e . The relation between this data is smooth and can be safely assumed that it can be captured by a polynomial relation of low degree (Eq. (15)).

3) We find the mathematical relationship, $C(\Lambda)$ between the Hamiltonian coefficient $\lambda_1 = m_e$ and the fitting parameters $C = [c_0^{I(Q)}, \dots, c_N^{I(Q)}]$ found in step 2. This is achieved by interpolating c_j^Q and c_j^I coefficients with two new polynomials of degree L with respect to m_e :

$$\tilde{c}_j^{Q(I)}(m_e) = \sum_{k=0}^L b_k^{Q(I)} m_e^k, \quad (15)$$

where $b_k^{Q(I)}$ are the polynomial coefficients. Referring again to Fig. 2, it can be seen that c_j^Q coefficients can be easily linked to the corresponding m_e value by such L^{th} degree polynomial (15).

4) Finally, we reconstruct the control pulses for an arbitrary value of \tilde{m}_e by using Eq. (15) to compute the coefficients $c_j^{I(Q)}$ of the control pulse polynomial and then evaluating the polynomials $y_{I(Q)}$ with Eq. (14) which are equal by definition to the control pulses $\epsilon_I(t)$ and $\epsilon_Q(t)$. The control pulses obtained with this procedure can be used in the real quantum device to implement the desired transformation.

The functioning of the CPR method is pictorially represented in Fig. 1. The marked lines are the control pulses for the 1s orbital of the Hydrogen atom expanded in the STO-2G basis set for different m_e values. It can be seen that they smoothly change as m_e increases. These controls represent the data-set needed by the CPR method to work, as described in the step 1. The dotted lines are, instead, the reconstructed control pulses obtained through the step 4 of the here presented CPR Method.

A. Numerical Considerations

In the previous section we did not specify the choices of the mesh and of the degrees of the polynomials. The choice is, in fact, quite free and depends on the precision required by the reconstruction method. A finer mesh offers greater precision in the reconstruction of controls but also requires the calculation of a greater number of controls in the first step of the CPR method.

In our analysis, the mesh extends from $m_e = 0.5$ to 3. This choice is based on the observation that below 0.5 the rate of change of the control pulses shape with respect to m_e becomes very high and hence the coefficients $c_j^{I(Q)}$ become very distant and difficult to interpolate. Moreover the system approaches a non-physical singular solution since the mass of the electron can not be zero. For m_e values above 3, instead, the variations become smaller and smaller (so much that for values greater than $m_e = 3$, the controls can be approximated with the ones associated with $m_e = 3$)

Similarly, also the degree N and L of the polynomials (15) and (14) can be freely chosen to obtain higher or lower accuracies.

We study the fidelity reached by the CPR method as function of these parameters, namely the coarseness of the mesh (i.e. the number of control pulses), the degree N of polynomial (14) and the degree L of (15). Tab. II shows the average fidelity for different combinations of mesh densities, N and L values. The average fidelity is defined as the average of the fidelities between the reconstructed and exact propagator, calculated for 20 equally spaced points within the m_e mesh.

For the subsequent analysis, the CPR method param-

Mesh elements: 5			
N\L	2	4	6
2	0.99616	0.99926	-
4	0.99591	0.99978	-
6	0.99596	0.99973	-
Mesh elements: 10			
N\L	2	4	6
2	0.99614	0.99913	0.99925
4	0.99705	0.99985	0.99999
6	0.99704	0.99985	0.99999
Mesh elements: 15			
N\L	2	4	6
2	0.99591	0.99910	0.99922
4	0.99712	0.99987	0.99999
6	0.99712	0.99987	0.99999

TABLE II: This table summarizes the average fidelity for different combination of the number of mesh elements, the degree N of Eq. (14) and degree L of Eq. (15). The element in the box is the first combination of such parameters that guarantees an average fidelity greater or equal to 0.99990 (with the lowest computational cost). This combination has been chosen for the analysis carried out in this work.

eters have been chosen to ensure that, on average, the fidelity between the reconstructed propagator and the exact propagator was greater than 0.99990 (since initially we imposed a fidelity for the optimized controls to be grater or equal than 0.99999). Referring again to Tab. II, we can identify the combinations of the parameters that produce the desired precision of the method with the lower values of the parameters, hence with the lower computational cost. As can be seen again in Tab II such configuration is the one in the box. Our combination consists in a mesh of 10 values (i.e. 10 controls), the degree N of the first polynomial (Eq. 14) equal to 4 and a degree L of the second polynomial (Eq. 15) equal to 6.

B. Test

To test the validity of our reconstruction procedure, we evaluate the fidelity Φ between the exact and the reconstructed control pulses short-time propagator. As anticipated in the previous section, we selected a combination of parameters that ensure a fidelity mean value of 0.99999, which is almost equal to what one would obtain through standard control optimization procedure.

Since the aim of this work is to find a method to enhance the performance of a simulation in which the short-time propagator parameters are, in turn, dependent on time, we set up a simulation in which at every time-step, t , the mass m_e is changed according to the equation: $m_e^t = 1.0 + 0.2 \sin(t\pi/N_{\max})$ for $t = \{0, 1, \dots, N_{\max}\}$, with N_{\max} an arbitrary number that we take equal to 50 in order to have a smooth plot. So we proceed, iteratively, by changing the mass, reconstructing the controls via CPR

method, computing the propagator and then applying it to advance the simulation. The results are presented in Fig. 3 and they show the time-dependent probabilities for the Hydrogen's electron to occupy one of the two element of the STO-2G basis. The solid lines represent the exact dynamics computed by the numerical integration of the Schrödinger equation (2), while the circles represent the quantum device's simulated output probabilities at the end of each control pulse application (starting from the previous time-step). We see that the quantum devices simulated evolution (circles) obtained by our CPR method, follows very closely the exact evolution. A performance gain estimate is obtained by comparing the average times required by the CPR method and the standard optimization algorithm to obtain a single control pulse. One step with CPR method takes on average 0.721 (± 0.002) seconds, while the optimization algorithm (GRAPE) takes on average 5.19 (± 0.02) seconds. The ratio between these times is 7.2, which means that the proposed method is, roughly, 7 times faster (in the device-level simulation framework with the parameters identified in Tab. II).

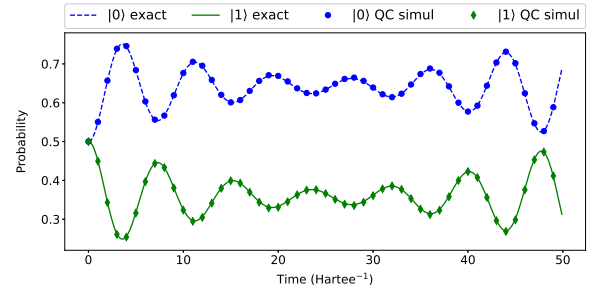


FIG. 3: Temporal evolution of 1s orbital of the hydrogen atom for cyclic variation of the electron mass m_e . The plot represents the probability that the qudit is in state $|0\rangle$ or $|1\rangle$ during the simulation. At every time-step the m_e value is changed, the control pulses relative to m_e are reconstructed via the CPR method and then used to advance the simulation. The propagator obtained through the reconstructed controls (circles) follows closely the exact evolution (lines).

V. CONTROL PULSE RECONSTRUCTION VIA FOURIER TRANSFORM (CPRFT) METHOD

So far we have considered cases for which the driving pulses resulting from the optimization procedure are rather simple, and can be directly fitted with an ad-hoc functional form. However, in general, the pulses have shapes that cannot be easily interpreted in terms of elementary functions, since they could contain multiple frequency components. A possible solution is to use an expansion over a basis set. In the general scheme presented in Sec. III, the step of fitting the pulse is then simply replaced by finding the expansion coefficients over

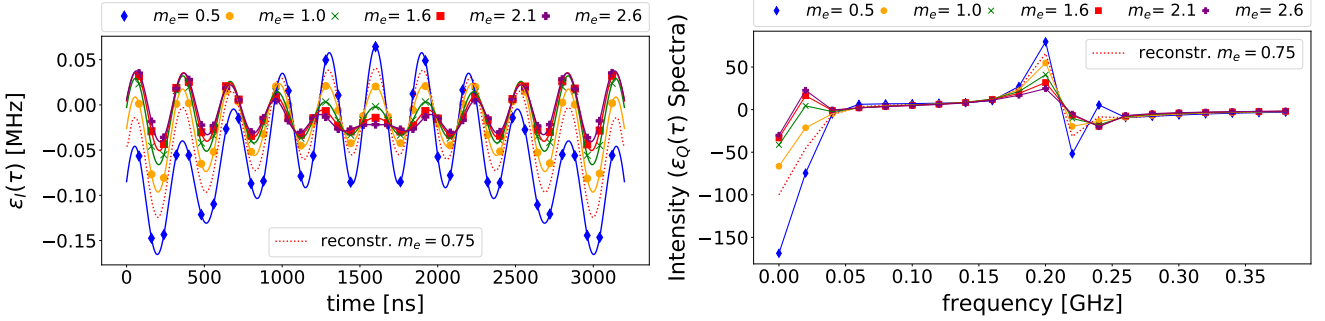


FIG. 4: Left panel: In-quadrature components of control pulses (ϵ_Q) as function of m_e , for short-time propagators of $1s$ orbital of the hydrogen atom expanded in the STO-3G basis. A family of smoothly varying function arise. Right panel: Spectra of the control pulses computed via Fourier transform. Also the spectra change smoothly.

the chosen basis. For periodic signals an obvious choice is that of operating a Fourier transform on each of the pulses $\epsilon_{Q(I)}(t)$. The resulting set of curves $\tilde{\epsilon}_{Q(I)}(\omega; C)$, which are the spectra of the control pulses, needs then to be interpolated as a function of $\Lambda = \lambda = m_e$, interpreting each frequency of the spectra as a component c_j of the coefficient vector C . A driving pulse for an arbitrary point in the parameter space can then be obtained by interpolating the corresponding spectrum and performing the inverse Fourier transform.

We applied this method to the same electron-mass dependent hydrogen atom. To have less trivial control pulses, we expanded the Hydrogen Hamiltonian on a STO-3G basis set (instead of STO-2G as in Sec. IV) and then we mapped the states of the system onto a 3 level transmon. The Hamiltonian is now given by a 3×3 matrix.

In Fig. 4, the control pulses $\epsilon_Q(t)$ for different m_e values for the 3 level system are presented. It can be seen that the controls present higher frequency components and the fitting method described in the previous sections would be of no use. However, also in this case one can still notice that a smoothly varying family of controls emerges.

Now, we Fourier transform the control pulses, obtaining a set of spectra, plotted in the right panel of Fig. 4. Each frequency of the spectrum changes smoothly as a function of the electron mass m_e . Hence, we can interpolate each component of the spectrum and reconstruct it for an arbitrary value of m_e . Once we obtain the new spectrum, we can transform it back to the time domain, obtaining finally the reconstructed control pulse.

These control pulses can now be used to directly implement a gate in the real quantum device or, in the case of our simulation, to reconstruct the propagator and use it in the device-level simulation.

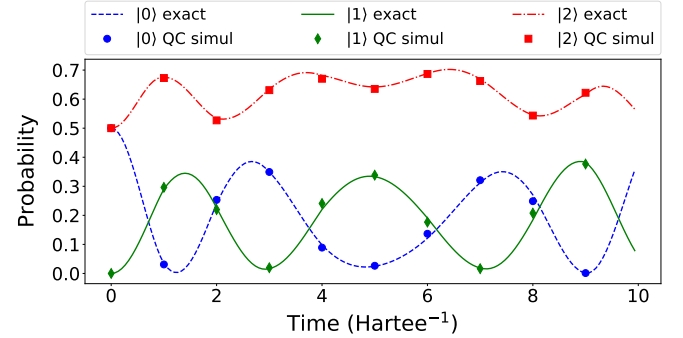


FIG. 5: Time-dependent occupation probabilities of the $1s$ hydrogen's orbital expanded onto STO-3G basis, starting from an initial arbitrary state. The lines represent the exact evolution obtained through the numerical solution of Eq. (2). Dots represent the quantum device simulated output obtained by, iteratively, changing the electron mass, reconstructing the control pulses via FTCPR method, computing the numerical propagator (via the right-hand side of (10)), and finally advancing the simulation with (3) (starting from the previous time-step). The agreement is very good.

Num. mesh elements	5	10	15	20
Num. spectra elements	71	40	40	40
Fidelity	0.89745	0.99823	0.99959	0.99985

TABLE III: CPRFT method average fidelities for meshes with a different number of elements and for spectra with a different number of elements taken into account. The fidelity in the box identifies the combination of parameters used in the analysis of Sec. V.

A. Numerical Consideration

Also in this case, some considerations on the precision of the method have to be made. The relevant parameters of the CPRFT method are the number of elements

in the m_e mesh (i.e. the number of controls) and the number of the elements of the spectra that one takes into account for the interpolation. Concerning the first parameter, the same considerations of the previous section hold. Regarding the last parameter, it is well known that the spectrum has twice the number of elements as the signal from which it derives. However, half of them are repeated and can be discarded in the analysis. Moreover, above certain frequencies, elements are very close to zero and can be neglected. We therefore truncate the spectrum to the lowest number of element which allows an accurate reconstruction of the signal. To achieve such result we simply neglect all the elements three order of magnitude smaller than the maximum values in the whole set of spectra. Moreover, we make sure that the length of the truncated spectra is the same for all, otherwise the interpolation between the spectra cannot be properly done.

In general, as in the previous case, we can study the fidelity as function of the FTCPR method's parameters. The result is shown in Tab. III. The average fidelity in the box represents the chosen parameters combination, since it guarantees a good fidelity (on average, greater than 0.9990) with the lower number of mesh elements possible, hence the lower computational cost. The configuration consists of 10 controls and of 40 spectra's components.

B. Test

The agreement between the exact solution and the solution provided by the CPRFT method is very good. As discussed in the previous subsection, the average fidelity is 0.9996. Although the addition of the third level and the use of a integral transform lowers the average fidelity of the method, its value is still at an acceptable level, also considering the computational speed-up.

Again, we simulate the system with a time dependent variation of the Hamiltonian parameter, m_e . We follow the same procedure of the previous section and we simulate the system changing at every time-step t the electron mass according to $m_e^t = 1.0 + 0.2 \sin(t\pi/N_{\max})$ for $t = \{0, 1, \dots, N_{\max}\}$, with N_{\max} an arbitrary number that we take equal to 50 in order to have a smooth plot. Fig. 5 shows the occupation probabilities for the usual hydrogen system expanded onto STO-3G. Also in this case we find a good agreement between the quantum device simulated output (circles) and the exact evolution obtained by numerical integration of Schrödinger equation (lines).

From the computational point of view, we again find a good improvement in the time required to obtain a single control pulse. The average time needed to compute a control pulse with the CPRFT method is 0.780 ± 0.002 seconds, while the GRAPE algorithm takes 11.1 ± 0.03 seconds. This means that the CPRFT method is roughly 14 times faster.

	STO-2G	STO-3G	STO-4G
GRAPE	$5.19 \pm 0.02s$	$11.13 \pm 0.03s$	$19.85 \pm 0.04s$
CPRFT	$0.780 \pm 0.002s$	$0.800 \pm 0.002s$	$0.743 \pm 0.002s$

TABLE IV: The average computational time for a single control pulse via GRAPE and the CPRFT method are shown. The time required by the optimization grows with the number of levels (i.e. the number of STO-NG basis elements) while the time required by CPRFT method remains constant and very low.

VI. SCALING AND COMPARISON

The scaling of the method is good and improves as the number of levels of the quantum device we consider increases. In Tab. IV the computing time for a single control with GRAPE and with CPRFT method is shown. The former grows as the number of levels increases, while the latter remains constant and one or two orders of magnitude smaller depending on the situation. If we extend the analysis to an arbitrary number of levels (or qubits), as shown in Fig. 6, it is evident that the computation time increases exponentially with the number of levels. Hence the CPRFT method, at least in principle, becomes more and more efficient as the number of levels increases.

The bottleneck of the CPRFT method is of course the requirement to compute a certain number of controls in advance. As pointed out in Sec. IV A and V A, the number of these control pulses is a parameter of primary importance. A high number of them will allows an excellent accuracy in the reconstruction of the control pulses, but it will also require a longer time, and vice-versa.

We can give a quantitative analysis of the scaling of the FTCPR method. Let t_c be the time needed to calculate a control with GRAPE, t_m the time needed with our method, N_{con} the number of control pulses to be calculated in advance and M_{con} the number of control pulses one wishes to reconstruct with the CPRFT method. The total time needed to compute M_{con} control pulses with the standard optimization procedure is $T_{\text{GRAPE}} = t_c M_{\text{con}}$. If, on the other hand, we use the CPRFT method, also taking into account the time needed to calculate all the N_{con} controls in advance, the total time becomes $T_{\text{CPRFT}} = t_c N_{\text{con}} + t_m M_{\text{con}}$. It is clear that we would have a computational advantage if $T_{\text{GRAPE}} < T_{\text{CPRFT}}$. As an example, we take $N_{\text{con}} = 50$, $M_{\text{con}} = 1000$, $t_c = 53s$ and $t_m = 0.78s$ obtaining a $T_{\text{GRAPE}} = 53000s = 14.7h$ and a $T_{\text{CPRFT}} = 2650 + 780 = 3430s = 0.95h$. In this case the reduction of total computation time is of two order of magnitude.

Concerning the fidelity scaling, from the Tab. V we note that the fidelity, for the same number of mesh elements, decreases approximately by an order of magnitude for each additional level. Up to the case with 4 levels (STO-4G) the fidelity is, however, very good with a small number of mesh elements and, furthermore, its reduction is compensated by a reduction in the computation time.

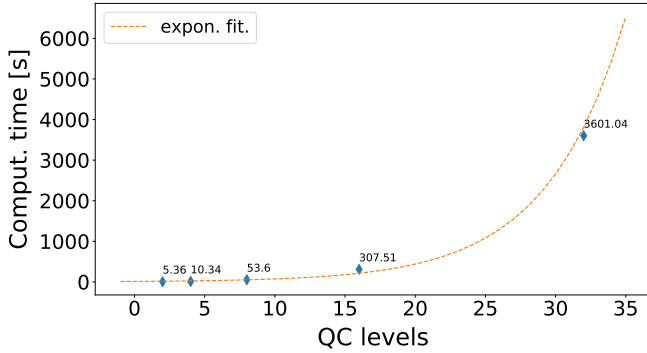


FIG. 6: Computational time vs. the number of level of a quantum device. The single time data (diamonds markers) are computed for 2^N QC levels with $N = [1, 2, 3, 4, 5]$ (which identify the total number of level for 1,2,3,4 or 5 standard qubits). Computational time grows exponentially with the number of levels, as exponential fitting highlights (dashed line).

STO-2G			
mesh elements	10	15	20
spectrum elements	24	24	24
fidelity	0.99983	0.99995	0.99999
STO-3G			
mesh elements	10	15	20
spectrum elements	68	66	66
fidelity	0.99823	0.99959	0.99995
STO-4G			
mesh elements	10	15	20
spectrum elements	168	184	132
fidelity	0.92286	0.94063	0.99924

TABLE V: The table shows the fidelity of the CPRFT method for different combination of mesh density and number of STO-NG basis element. The fidelity decreases by an order of magnitude for each additional basis element. The fidelity is, however, still at an acceptable level considering also the computational time speed-up. Clearly, the loss of fidelity could be compensated by increasing the number of mesh elements.

VII. CONCLUSION

We introduced a general scheme, the Control Pulse Reconstruction (CPR) method, that can be used to increase the performance of quantum computations based on optimal control techniques whenever a frequent evaluation of the control pulses is needed. In general this corresponds to consider a family of Hamiltonians or propagators that are dependent by some parameter, which is, in turn, a function of the evolution time. As a test of this protocol, we presented the simulation of the real time evolution of the electron wave function of the hydrogen atom mapped on a controllable multi-level superconducting qubit. The 1s orbital state of the hydrogen atom was

expanded in the STO-2G and STO-3G basis. The control pulses for the single multi-level gate, necessary to encode the propagator onto the quantum device, was obtained by a numerical optimization using the GRAPE algorithm as implemented in the QuTiP python package. By calculating a set of control pulses of propagators which differ in the value of a parameter and, then, finding a functional dependence between the shape of these control pulses, it was possible to derive a mathematical model that allows to reconstruct the control pulses of an arbitrary value of the parameter bypassing the numerical optimization. We showed results for two realizations of this procedure. A first simple one makes use of polynomial fitting. A more complex one uses, instead, the fit of the control pulse spectra meant to interpolate periodic pulses of arbitrary shape. To investigate the performance of our approach we computed the fidelity between the exact and the reconstructed propagator, obtaining in all cases excellent results. We also presented a simulation of the hydrogen Hamiltonian in both STO-2G and STO-3G expansion, with a time-dependent electron effective mass, for which we showed that the time required to perform the simulation with our method is one order of magnitude smaller than the original approach (in the device-level quantum simulations). Complex systems whose Hamiltonian depends on some external parameters require the control pulses to be optimized at every time-step. So this method, avoiding the great amount of time and computational resources needed for the computation, could be of great interest to improve the quantum systems simulation of realistic systems. More complex situations, as the study of nucleon spin dynamics, could indeed strongly benefit of this method. In particular, it opens the possibility for a manageable implementation of several classical-quantum co-processing protocols.

VIII. ACKNOWLEDGMENT

This research was partially supported by Q@TN grants ML-QForge (PL) and ANuPC-QS (FT). This work was prepared in part by LLNL under Contract DE-AC52-07NA27344 with support from the Laboratory Directed Research and Development grant 19-DR-005.

Appendices

A. HYDROGEN ATOM IN THE STO-KG BASIS

The s-wave Hydrogen atom in spherical coordinates is given by:

$$H_{hy} = \left[-\frac{\hbar^2}{2m_e} \left(\frac{d^2}{dr^2} + \frac{2}{r} \frac{d}{dr} \right) - \frac{e^2}{r} \right], \quad (16)$$

where m_e , \hbar , and e are, respectively, the electron mass, the reduce Planck constant and the electron charge, here

K	i	A_i	α_i
2	1	0.6789	0.1516
	2	0.4301	0.8518
3	1	0.4446	0.1098
	2	0.5353	0.4057
	3	0.1543	2.2276
4	1	0.2916	0.0880
	2	0.5328	0.2652
	3	0.2601	0.9546
	4	0.0567	5.2168

TABLE VI: Values of A_i and α_i for the $1s$ orbital of the hydrogen atom (Eq. 20) in the STO-KG basis with $K = 2, 3, 4$.

used in the atomic units (and so, from now on, set to 1 unless otherwise specified). The ground state energy of this Hamiltonian is -0.5 Hartree.

In order to solve the Schrödinger equation describing the dynamics of the electron, we expand the electron $1s$ orbital on a set of given basis functions, following the standard procedures used in computational chemistry [16]. There are two common choices for the basis function sets: The Slater type orbitals (STO), and the Gaussian type orbitals (GTO). STO have the general form:

$$B_{n,l,m,\zeta}(r, \theta, \phi) = NY_{l,m}(\theta, \phi)r^{n-1}e^{-\zeta r}, \quad (17)$$

while GTO have the general form:

$$B_{n,l,m}(r, \theta, \phi) = NY_{l,m}(\theta, \phi)r^{2n-2-l}e^{-\zeta r^2}, \quad (18)$$

where N is a normalization constant, n, l, m are, respectively, the principal quantum number, the azimuthal quantum number and the magnetic quantum number and $Y_{l,m}$ are spherical harmonics. In general, STO basis functions better represent the orbitals shape, having the cor-

rect asymptotic behaviour, but GTO are less computationally intensive. A compromise solution is to use a sum of K GTO function to approximate each STO function of a given basis. This originates the STO-KG basis set. STO-KG orbitals have the following general form [26]:

$$B_{n,l,m,\zeta}(r, \theta, \phi) = Z(r, \theta, \phi) \sum_{i=1}^K A_i \left(\frac{2\alpha_i}{\pi} \right)^{\frac{3}{4}} e^{-\alpha_i r^2}, \quad (19)$$

where $Z(r, \theta, \phi) = NY_{l,m}(\theta, \phi)r^{2n-2-l}$, K is the number of GTO functions used in the expansion and A_i and α_i are numerical parameters obtained by a variational procedure [26]. Some of them, also used in the present work, are reported in Tab. VI.

In general, atomic and molecular orbitals are represented by a sum of an adequate number of basis element in order to obtain a good approximation of the complete orbital and a good precision in the computation. For our investigation we only need to approximate the $1s$ orbital so we need only one of this basis. We therefore set $n = 1$ and $l = m = 0$, so that $Y_{0,0}$ is constant and it can be neglected. Finally, the hydrogen wavefunction can be written as:

$$|\psi(r)\rangle = \sum_{i=1}^K A_i \left(\frac{2\alpha_i}{\pi} \right)^{\frac{3}{4}} e^{-\alpha_i r^2}. \quad (20)$$

Finally we can compute the numerical Hamiltonian (16) by computing the expected result as:

$$H = \langle \psi(r) | H_{hy} | \psi(r) \rangle \quad (21)$$

or, in discrete form:

$$H_{i,j} = \langle \phi_i | H_{hy} | \phi_j \rangle \quad (22)$$

with $\phi_i = A_i \left(\frac{2\alpha_i}{\pi} \right)^{\frac{3}{4}} e^{-\alpha_i r^2}$

This Hamiltonian form allows for a one-to-one mapping between GTO basis functions the levels of the qudit (3D transmon).

[1] C. Dawson and M. Nielsen, *Quantum Information and Computation* **6** (2005), 10.26421/QIC6.1-6.

[2] D. P. DiVincenzo, Fortschritte der Physik: Progress of Physics **48**, 771 (2000).

[3] R. Barends, L. Lamata, J. Kelly, L. García-Álvarez, A. Fowler, A. Megrant, E. Jeffrey, T. White, D. Sank, J. Mutus, *et al.*, Nature communications **6**, 1 (2015).

[4] A. P. Place, L. V. Rodgers, P. Mundada, B. M. Smitham, M. Fitzpatrick, Z. Leng, A. Premkumar, J. Bryon, S. Sussman, G. Cheng, *et al.*, arXiv preprint arXiv:2003.00024 (2020).

[5] A. Nersisyan, S. Poletto, N. Alidoust, R. Manenti, R. Renzas, C.-V. Bui, K. Vu, T. Whyland, Y. Mohan, E. A. Sete, *et al.*, (2019).

[6] L. B. Nguyen, Y.-H. Lin, A. Somoroff, R. Mencia, N. Grabon, and V. E. Manucharyan, Physical Review X **9**, 041041 (2019).

[7] J. P. Palao and R. Kosloff, Physical review letters **89**, 188301 (2002).

[8] Y. Atia, Y. Elias, T. Mor, and Y. Weinstein, International Journal of Quantum Information **12**, 1450031 (2014).

[9] E. T. Holland, K. A. Wendt, K. Kravvaris, X. Wu, W. E. Ormand, J. L. DuBois, S. Quaglioni, and F. Pederiva, Physical Review A **101**, 062307 (2020).

[10] J. Chow, L. DiCarlo, J. Gambetta, F. Motzoi, L. Frunzio, S. Girvin, and R. Schoelkopf, arXiv preprint arXiv:1005.1279 (2010).

[11] X. Wu, S. L. Tomarken, N. A. Petersson, L. A. Martinez, Y. J. Rosen, and J. L. DuBois, Physical Review Letters **125**, 170502 (2020).

[12] J. Werschnik and E. Gross, Journal of Physics B: Atomic, Molecular and Optical Physics **40**, R175 (2007).

[13] S. Kirchhoff, T. Keßler, P. J. Liebermann, E. Assémat, S. Machnes, F. Motzoi, and F. K. Wilhelm, Physical Review A **97**, 042348 (2018).

[14] S. Machnes, U. Sander, S. J. Glaser, P. De Fouquière, A. Gruslys, S. Schirmer, and T. Schulte-Herbrüggen, Physical Review A **84**, 022305 (2011).

[15] P. J. J. O’Malley, R. Babbush, I. D. Kivlichan, J. Romero, J. R. McClean, R. Barends, J. Kelly, P. Roushan, A. Tranter, N. Ding, B. Campbell, Y. Chen, Z. Chen, B. Chiaro, A. Dunsworth, A. G. Fowler, E. Jeffrey, E. Lucero, A. Megrant, J. Y. Mutus, M. Neeley, C. Neill, C. Quintana, D. Sank, A. Vainsencher, J. Wenner, T. C. White, P. V. Coveney, P. J. Love, H. Neven, A. Aspuru-Guzik, and J. M. Martinis, *Phys. Rev. X* **6**, 031007 (2016).

[16] F. Jensen, *Introduction to computational chemistry* (John wiley & sons, 2017).

[17] H. Paik, D. I. Schuster, L. S. Bishop, G. Kirchmair, G. Catelani, A. P. Sears, B. R. Johnson, M. J. Reagor, L. Frunzio, L. I. Glazman, S. M. Girvin, M. H. Devoret, and R. J. Schoelkopf, *Phys. Rev. Lett.* **107**, 240501 (2011).

[18] J. Koch, T. M. Yu, J. Gambetta, A. A. Houck, D. I. Schuster, J. Majer, A. Blais, M. H. Devoret, S. M. Girvin, and R. J. Schoelkopf, *Phys. Rev. A* **76**, 042319 (2007).

[19] M. Kjaergaard, M. E. Schwartz, J. Braumüller, P. Krantz, J. I.-J. Wang, S. Gustavsson, and W. D. Oliver, Annual Review of Condensed Matter Physics **11** (2019).

[20] N. Khaneja, T. Reiss, C. Kehlet, T. Schulte-Herbrüggen, and S. J. Glaser, Journal of magnetic resonance **172**, 296 (2005).

[21] B. Rowland and J. A. Jones, Philosophical Transactions of the Royal Society A: Mathematical, Physical and Engineering Sciences **370**, 4636 (2012).

[22] A. Blais, A. L. Grimsmo, S. M. Girvin, and A. Wallraff, *Rev. Mod. Phys.* **93**, 025005 (2021).

[23] A. Blais, A. L. Grimsmo, S. Girvin, and A. Wallraff, arXiv preprint arXiv:2005.12667 (2020).

[24] H.-L. Huang, D. Wu, D. Fan, and X. Zhu, Science China Information Sciences **63**, 1 (2020).

[25] J. R. Johansson, P. D. Nation, and F. Nori, Computer Physics Communications **184**, 1234 (2013).

[26] W. J. Hehre, R. F. Stewart, and J. A. Pople, The Journal of Chemical Physics **51**, 2657 (1969).